Supplementary Data for:

Single and Double Box HMGB Proteins Differentially Destabilize Nucleosomes

Micah J. McCauley[1*], Ran Huo[1*], Nicole Becker[2], Molly Nelson Holte[2], Uma M. Muthurajan[3], Ioulia Rouzina[4], Karolin Luger[3,5], L. James Maher III[2], Nathan E. Israeloff[1], Mark C. Williams[1#]

[1]*Department of Physics, Northeastern University, Boston, Massachusetts, USA.*
[2] *Department of Biochemistry and Molecular Biology, Mayo Clinic College of Medicine and Science, Rochester, Minnesota, USA.*
[3] *Department of Chemistry and Biochemistry, University of Colorado, Boulder, Colorado, USA.*
[4] *Department of Chemistry and Biochemistry, Ohio State University, Columbus, OH, USA.*
[5] *Howard Hughes Medical Institute, Chevy Chase, MD, USA.*

[*]Contributed equally to this work.

[#]To whom correspondence should be addressed, Email: mark@neu.edu

Supplement Outline

Supplementary Methods 1. Dual Gaussian fits.

Once a height threshold is determined for an array (see Supplementary Figure S1 for a sample), each core particle is identified and the distance to the nearest neighboring particle measured (the linker DNA is not reliably visible in these images). The distributions of nearest neighbor distances (Figure 2) are well fit to a dual Gaussian equation:

$$f(x) = a_1 e^{\frac{(x-\mu_1)^2}{2\sigma_1^2}} + a_2 e^{\frac{(x-\mu_2)^2}{2\sigma_2^2}}. \quad \text{(S1)}$$

The implications of these two distances are discussed further below (Supplementary Figure S2). For each fit shown in Figure 2, Supplementary Figure S3 and S4, distributions of nucleosome distances are observed in varying concentrations of HMGB protein for the number of arrays (*n*) shown, giving a total number of nearest neighbor distances (*N*, also the number of core particles observed). Measured distances are cut off below ~10 nm (corresponding to nucleosomes significantly stacked upon each other) and above 75 nm (or 220 base pairs, corresponding to fully released core particles). Typically, less than 1% of the identified core particles lay beyond these boundaries. However, in 0.3 nM Hmo1, over 5% of the nucleosomes are beyond 75 nm away, due to significant unwinding (and likely complete tetramer release) caused by this protein. Fits are minimized in Excel and calculated χ_v^2 values are between 0.5 and 2. Each fit returns a pair of mean distances (μ), standard deviations (σ) and amplitudes (a). Typical fits are shown in Figure 2G, 3E and 3F and the complete sets are in Supplementary Figure S3 and S4. Reported errors in the fitted distances are shown in Figure 3 and reflect the standard error in the mean (one sigma), as found by variations in χ_v^2 (1).

Distinct mean distances indicate two different geometries of nearest neighbors that are found on the surface, as discussed in the main text. Briefly, the distribution of larger nearest neighbor distances indicates core particles that are sequential along the DNA. The stiffness of the rigid linker DNA effectively adds that length to the center-to-center distance. Non-sequential core particles tend to lie closer together on the mica surface. The mean distances in the presence of Hmo1 and Nhp6A are summarized in Figure 3G and 3H. The standard deviations of the two distributions do not appear to show meaningful variations across protein concentration within the uncertainty of the fitted results. Finally, the amplitudes should be simply related to the standard deviations for a normal distribution. However, in these experiments the amplitudes also reflect the relative number of sequential and non-sequential particles identified on the surface.

At high concentrations (as *c* approaches the K_d of protein binding to bare DNA), array condensation is visible and the distinction between sequential and non-sequential distances becomes lost. Furthermore, stacking of core particles becomes evident, as shown in Supplementary Figure S5.

Supplementary Methods 2. Modeling observed AFM length distributions.

A simple model of nucleosome unwrapping predicts core particle positions on the AFM surface, with the additional advantage of exact knowledge of the sequential nucleosome positioning. Nucleosome dimensions are assumed as shown in Figure 1; each core particle forms a disk of diameter d = 11 nm separated by linker DNA of length ℓ_o = 20 nm (60 base pairs). The remaining 147 base pairs are wrapped

around ~1.8 turns. Since linker lengths are substantially less than the persistence length of DNA (50 nm, or 150 base pairs), these segments are assumed to be straight and to enter and exit the nucleosome tangentially to the disk. Following the backbone, the entry and exit DNA form an angle at each core particle of β_o = 80°. If a length of DNA ($\Delta\ell$) unwraps from each particle, then the center distance between successive core particles, ℓ , may be simply written (ignoring the diameter of each nucleosome which introduces only a small correction shown in Figure 3C);

$$\ell = \ell_o + \Delta\ell \,. \tag{S2}$$

Unwinding also changes the angle between the entry and exit linker DNA;

$$\beta = \beta_o + \Delta\beta + \left(\frac{360^\circ}{75bp}\right)\cdot\Delta\ell - 180^\circ \cdot P_f \,. \tag{S3}$$

An additional term allows additional DNA flexibility at the entry points ($\Delta\beta$), and a probability of core particle flipping (P_f).

To construct a pseudo-image of an 12x nucleosome array, each nucleosome position is calculated in sequence (starting from an origin) per values using Supplementary Equations S2 and S3, with random variations allowed in angle ($\Delta\beta$) and length ($\Delta\ell$). For each array image, the set of sequential distances is recorded, while the nearest neighbor is also found. This data is randomly generated for 42 arrays, then each set of distances is analyzed and fit exactly as the AFM data of the main text (described above). In practice, physically reasonable variations in angle ($\Delta\beta < 90^\circ$) do not meaningfully change the array distributions, while variations in unwrapping length coupled with a probability of core particle flipping, do. So, for what follows, $\Delta\beta$ is set to zero. Finally, the distribution in the unwrapping length is assumed to be flat (non-Gaussian), and the probability of flipping was fixed at P_f = 0.5, for simplicity.

Due to these simplifications, the following simulations are not meant to quantitatively reproduce the exact set of sequential nucleosome distances. However, variations in the unwrapped DNA length do allow these simulations to qualitatively match the AFM data measured in the main text. For a single array, the trivial case corresponds to no unwrapping or flipping allowed ($\Delta\ell$ and P_f = 0), leading to a ring of nucleosomes ~30 nm in diameter, with some stacking (this is not the same structure as the H1 mediated 30 nm fiber). However, in an AFM image nearly all disks are flat on the surface. This implies that both some disk flipping and unwinding must take place. A good match for the data of the main text (Fig. 2, and Fig. S3 and S4) may be made by choosing $\Delta\ell$ = 20 nm (while P_f = 0.5 for all simulations that follow). The set of 42 arrays shown in Fig. S5 reproduces the key features of the measured AFM data.

According to panel A) and B) of Figure S2, the measured nearest neighbor distances cannot recover all of the linker lengths, and the measured distances fall into two distributions; a longer length corresponding to the correct sequential linker lengths recovered and a short length corresponding to non-sequential distances. Gaussian fitting to these sequential lengths (Supplementary Equation S1) is a reasonable proxy for the actual linker lengths. The measured average sequential distance is found to be 22 ± 3 nm, while most of the unwound nucleosomes are found to lie closer to non-sequential neighbors. However, the width of the fitted distribution does match the measured data, indicating that some DNA must unwind, and some nucleosomes have H2A/H2B contacts with the DNA that are broken, even in the absence of protein.

In the presence of 5 nM of Nhp6A, the AFM data becomes difficult to fit and shows multiple local minima. When $\Delta\ell$ now chosen to be 40 nm, the distribution matches the data well (Fig. S5). Now the fitted value of 32 ± 4 nm for the sequential neighbors is the same as the AFM data shown in Fig. S4. Furthermore, the qualitative fit obtained by simply unwrapping the nucleosome with the same amount of fraying, so that ℓ_o = 40 nm and $\Delta\ell$ = 20 nm is poor (Fig S5). Now two distinct peaks are clearly visible, one each for the sequential and non-sequential distances, compared to a large non-sequential and a broad sequential length distribution actually seen in the AFM data.

These simulations reveal that for some nucleosomes even in the absence of protein, DNA unwinding leads to the loss of the H2A/H2B contact, and this leads to the distribution of sequential distances seen in the AFM data. These distances represent the recovered linker lengths along the DNA, though the fitted peak of the AFM data may underestimate unwinding, as some unwound DNA is counted as non-sequential. Furthermore, these results support the key result; adding Nhp6A measurably increases the average degree of unwinding, while Hmo1 increases it further. Finally, these simulations point to a strong degree of heterogeneity in unwinding in these AFM experiments.

Supplementary Methods 3. Quantifying DNA elasticity.

The end-to end length of DNA is affected by a force-dependent elasticity which influences all the distances measured in this work. This elasticity is typically described by an elastic continuum polymer model known as the worm-like chain, where the observed length per base pair of the polymer is dependent on the applied force $b(F)$ (2):

$$b(F) = B\left[1 - \frac{1}{2}\left(\frac{k_B T}{PF}\right)^{1/2} + \frac{F}{S}\right]. \qquad \text{(S4)}$$

The contour length B is the end to end length traced along the chain, and the elastic modulus S is also a longitudinal enthalpic stretch modulus. A measure of the entropic lateral elasticity is the persistence length P, which is an average segment length along the chain where the directional vector does not vary by more than one radian. The persistence length is typically 50 nm, or about 150 base pairs. DNA sequences that are shorter, such as the 60 base pair linkers of this study, may be effectively modeled as straight segments, as stated in the main text.

Extension/release data may be fit to Eq. S4 and for long (48,500 bp) phage-λ DNA this model gives distinctive values of B = 0.340 ± 0.001 nm/bp, P = 49 ± 3 nm and S = 1200 ± 200 pN (3,4). Furthermore, DNA-binding ligands may be introduced and changes in the fitted parameters will determine the extent of protein binding. Specifically, for this work, changes to the persistence length serve as a marker of protein binding and this will allow us to characterize binding to linker DNA in nucleosome arrays.(2,3).

Cycles of extension/release are examined for the shorter construct (5200 bp) used here, but in the absence of nucleosomes. Non-linear fits utilize custom LabWindows CVI which incorporated a ML Numerical Recipes algorithm ($\chi_\nu^2 \sim 1$ for all fits) (1). Measurements for n = 14 control DNA constructs determine P = 49.3 ± 0.8 nm, including a correction for the finite chain length and the presence of the tethering beads (5). Varying concentrations of HMGB proteins, with $n > 4$ at each concentration give results also shown in Figure 5G and 5H and are compared to previous results as described below.

Supplementary Methods 4. Characterizing HMGB binding in AFM experiments.

The AFM experiments in this work show that HMGB binding both disperses and compacts DNA under different protein concentrations. Experimental results and simulations above show that dispersion is driven by the disruption of DNA-histone interactions due to DNA-HMGB binding. Array compaction occurs as HMGB binds to linker DNA, increasing the flexibility of otherwise straight sections of DNA and allowing the array of HMGB-DNA-histones to condense. As these binding sites are separate and non-interacting, we may quantify binding with a simple model of two independent binding events, which contribute to the nearest neighbor length:

$$\begin{aligned}\ell &= \ell_o + \Delta\ell_d\left(\theta_d\right) - \Delta\ell_c\left(\theta_c\right) \\ &= \ell_o + \Delta\ell_d \cdot \frac{\left(c/K_d^{NCP}\right)^h}{1+\left(c/K_d^{NCP}\right)^h} - \Delta\ell_c \cdot \frac{\left(c/K_d^{DNA}\right)^h}{1+\left(c/K_d^{DNA}\right)^h} \quad .\end{aligned} \tag{S5}$$

Our previous studies fully characterized the binding of HMGB to DNA for both Nhp6A (3) and Hmo1 (4). The binding affinities for DNA and these HMGB proteins are summarized in Table 1, with an additional correction for finite handle bead sizes as shown previously (5). To reduce the number of free parameters, we may fix known values of the binding affinity K_d^{DNA} for Nhp6A and Hmo1 of 70 ± 10 nM and 3 ± 1 nM, while also fixing the array linker length ℓ_o at 24 nm, consistent with the value absent HMGB protein measured in the text. The length change upon compaction $\Delta\ell_c$ is fixed so that the average measured length at very large protein concentrations becomes simply the core particle diameter. Finally, the Hill parameter *h* is fixed at 2, set for protein binding that has been observed to be weakly cooperative (3,4). The fits appear in Figure 3G and 3H and return values for K_d^{NCP} of 1.8 ± 0.6 nM for Nhp6A and 0.09 ± 0.04 nM for Hmo1. The dispersion driven length change $\Delta\ell_d$ is 12 ± 2 nm for Nhp6A and 24 ± 3 nm for Hmo1, within uncertainty of the values determined by the peak experimental values of the mean separation. Finally, the values of χ_ν^2 return ~2, for Nhp6A and ~3 for Hmo1. Values are summarized in Table S1 and the values of K_d^{NCP} are also shown in Table 1 of the main text.

The final fits are not sensitive to the fixed values, except for the binding affinity of Nhp6A for DNA, which is reduced from 70 nM to 10 nM, to improve the quality of the fit (and this still only weakly affects the main parameter of interest, K_d^{NCP}). The discrepancy between these values is largely due to the lack of data at protein concentrations near K_d^{DNA}. These errors would improve if more data could be collected at higher protein concentration, though this would be experimentally difficult, as noted in the text.

Supplementary Methods 5. Characterizing HMGB-nucleosome binding in OT experiments.

The OT experiments in this work show that HMGB binding disrupts the histone-DNA contacts within the nucleosomes. At higher protein concentrations, direct binding to linker DNA is evident as a decrease in the persistence length and this drives array compaction. Since the decrease in the nucleosome disruption force and the change in the persistence length of DNA may be verified separately, they may also be fit separately.

HMGB binding to the nucleosome leads to a measured decrease in the force (F) measured at each disruption event seen in Figure 4D and 5A. Averaged over each nucleosome in the array, F_{avg} may be used to characterize the strength of HMGB binding according to a simple model:

$$F_{avg} = F_{NCP} - \left(F_{NCP} - F_{HMG}\right) \cdot \frac{\left(c/K_d^{NCP}\right)^h}{1+\left(c/K_d^{NCP}\right)^h}. \quad \text{(S6)}$$

The average force in the absence of HMGB proteins was found in the text to be F_{NCP} ~ 21 pN, which is left fixed as is the Hill parameter at a value of 2, to be consistent with the value in the AFM fits. These fits determine values for K_d^{NCP} of 1.6 ± 0.2 nM for Nhp6A and 0.29 ± 0.05 nM for Hmo1. The average force decreases to protein saturated values (F_{HMG}) of 9.3 ± 0.6 pN and 7.6 ± 0.6 nM for Nhp6A and Hmo1. While χ_v^2 ~1.7 for Nhp6A it is higher at ~8.6 for Hmo1. These values are summarized in Table S1 and the binding constants are also compared to the AFM results in Table 1 of the main text. The fits appear explicitly in Figure 5B and 5C.

Supplementary Methods 6. Charge screening during DNA-nucleosome unbinding.

The OT experiments in the main text quantify the stability of DNA-nucleosome interactions by measuring the average force during the disruption of the tetramer-DNA interactions (the inner turn). This average force is quantified in Figure 5B and 5C. In Figure 5E, we show the influence of changing solution conditions upon this force; in 100 mM Na^+, F_{avg} = 20.6 ± 0.3 pN, which increases to 27.6 ± 1.0 pN in 7.5 mM Na^+ (the buffer also changes from 10 mM HEPES to 10 mM Tris, but this does not contribute to the solution ionic strength and should not significantly affect the force). This increase reflects the stronger binding of DNA for the histones as the counterion concentration decreases. There is a similar increase in the force in the presence of saturating concentrations of Nhp6A (5 nM); F_{avg} = 10.3 ± 0.4 pN increases to 19.5 ± 1.0 pN in decreasing salt. This similar increase in force is consistent with the similar length of DNA released from the tetramer during these experiments.

The height of the energy barrier to force-induced nucleosome release ($G^\dagger$), estimated in Table S1, is affected by a change in counterion concentration;

$$\delta G_{el}^\dagger = \delta\left(F \cdot x^\dagger\right) = k_B T \cdot \delta Z^\dagger \cdot \ln\left[Na_2^+ / Na_1^+\right]. \quad \text{(S7)}$$

The change in the barrier height ($\delta G_{el}^\dagger$) is due to the change in [Na^+], while $\delta Z^\dagger$ is the change in the number of counterions during the rate limiting step of DNA ripping from the histone core. The measured change in the force (F) is determined from F_{avg} shown above. The distance to the transition state ($x^\dagger$) is derived from fits to Eq. 1. In 100 mM Na+, this value is 0.94 ± 0.10 nm and 0.60 ± 0.10 nm in 5 nM Nhp6A (Table S2), and in 7.5 mM Na+, this value is 0.66 ± 0.10 nm and 0.36 ± 0.10 nm in 5 nM Nhp6A (fits not shown). Now we may rearrange Eq. S7 to find $\delta Z^\dagger$;

$$\delta Z^\dagger = \frac{F_2 \cdot x_2^\dagger - F_1 \cdot x_1^\dagger}{k_B T \cdot \ln\left[Na_2^+ / Na_1^+\right]} \quad \text{(S8)}$$

As OT experiments on nucleosomes are moved from 100 mM Na^+ to 7.5 mM Na^+, the change in the number of counterions becomes δZ^+ = 0.11 $\pm$ 0.02 and when the nucleosomes are exposed to 5 nM Nhp6A and the salt is changed, the change is δZ^+ = -0.09 $\pm$ 0.03 per base pair. Without HMGB, there is a small association of Na^+ cations to the system, due to DNA unbinding from the histones. In the presence of HMGB, there is a slight negative change in the number of ions, possibly due to tighter HMGB binding after ripping, which would lead to some Na^+ expulsion. Though both proteins studied here show similar destabilization in high salt, the effect due to the single box Nhp6A is slightly weaker. So the change in the number of counterions should be somewhat greater with the addition of Hmo1.

Overall, the change in the ripping force with salt appears similar with or without HMG, and the distance to the transition state decreases with addition of HMG quite significantly, as does the change in the average number of Na^+ associating with the whole system during the rate limiting step of ripping. This indicates that the unbinding pathway stays the same in both high and low salt. Protein binding to DNA at the nucleosome exit or entry leads to protein invasion into DNA strong binding site, resulting in the less of the DNA needed to be unwound to rip DNA off this strong site, and less of the Na^+ cations associating with the system, consistent with the HMG protein neutralizing most of the charge of the DNA at the binding site.

Supplementary Methods 7. Characterizing HMGB-DNA binding in OT experiments.

HMGB binding to DNA has been well characterized for these proteins before (3,4) and here we only wish to show that the data compares reasonably to those works. A simplified model for the measured decrease in the persistence length should show a decrease from the value for DNA (P_{DNA}) to that of the DNA saturated with protein (P_{HMG}) according to:

$$P = P_{DNA} - \left(P_{DNA} - P_{DNA}\right) \cdot \frac{\left(c/K_d^{DNA}\right)^h}{1+\left(c/K_d^{DNA}\right)^h}. \qquad \text{(S9)}$$

The values of these parameter are all held fixed at the values shown in Table S1 (from the previous references) within uncertainty, though the value of K_d^{DNA} is changed slightly to 1 nM for Hmo1, noting, as above, the difficulty determining this value at low concentrations. Comparisons to the measured data appear in Figures 5G and 5H, and reinforce a key conclusion; K_d^{NCP} and K_d^{DNA} are measurably distinct, differing by a factor of 20x, and while binding to the nucleosome induces dispersion due to DNA release, DNA binding induces array compaction due to increased linker flexibility.

References

1. Press, W.H., Teukolsky, S.A., Vetterling, W.T. and Flannery, B.P. (2002) Numerical Recipies in C: The Art of Scientific Computing. Cambridge University Press, Cambridge.
2. Chaurasiya, K.R., Paramanathan, T., McCauley, M.J. and Williams, M.C. (2010) Biophysical characterization of DNA binding from single molecule force measurements. *Phys. of Life Rev.*, **7**, 299-341.
3. McCauley, M.J., Rueter, E.M., Rouzina, I., Maher, L.J., 3rd and Williams, M.C. (2013) Single-molecule kinetics reveal microscopic mechanism by which High-Mobility Group B proteins alter DNA flexibility. *Nucleic Acids Res.*, **41**, 167-181.
4. Murugesapillai, D., McCauley, M.J., Huo, R., Nelson Holte, M.H., Stepanyants, A., Maher, L.J., 3rd, Israeloff, N.E. and Williams, M.C. (2014) DNA bridging and looping by HMO1 provides a mechanism for stabilizing nucleosome-free chromatin. *Nucleic Acids Res.*, **42**, 8996-9004.
5. Seol, Y., Li, J., Nelson, P.C., Perkins, T.T. and Betterton, M.D. (2007) Elasticity of Short DNA Molecules: Theory and Experiment for Contour Lengths of 0.6–7 μm. *Biophys. J.*, **93**, 4360-4373.
6. Brower-Toland, B.D., Smith, C.L., Yeh, R.C., Lis, J.T., Peterson, C.L. and Wang, M.D. (2002) Mechanical disruption of individual nucleosomes reveals a reversible multistage release of DNA. *Proc. Natl. Acad. Sci. U. S. A.*, **99**, 1960-1965.
7. Evans, E. (2001) Probing the relation between force--lifetime--and chemistry in single molecular bonds. *Annu. Rev. Biophys. Biomol. Struct.*, **30**, 105-128.
8. van Holde, K. and Zlatanova, J. (1999) The nucleosome core particle: does it have structural and physiologic relevance? *Bioessays*, **21**, 776-780.
9. Hazan, N.P., Tomov, T.E., Tsukanov, R., Liber, M., Berger, Y., Masoud, R., Toth, K., Langowski, J. and Nir, E. (2015) Nucleosome Core Particle Disassembly and Assembly Kinetics Studied Using Single-Molecule Fluorescence. *Biophys. J.*, **109**, 1676-1685.

	P [1] (nm)	K_d^{DNA} [1] (nM)	$\Delta\ell_d$ [2] (nm)	K_d^{NCP} [2] (nM)	F_{avg} [3] (pN)	K_d^{NCP} [3] (nM)
DNA	50 ± 1	-	0	-	20.6 ± 0.3	-
DNA +Nhp6A	7 ± 0.5	70 ± 10	12 ± 2	1.8 ± 0.6	9.3 ± 0.6	1.6 ± 0.2
DNA +Hmo1	8 ± 0.5	3 ± 1	24 ± 3	0.09 ± 0.04	7.6 ± 0.6	0.29 ± 0.05

Supplementary Table S1. Binding affinity of HMGB in AFM and OT experiments.

1. The persistence length of DNA and the persistence length in the presence of HMGB proteins (at saturating concentrations) as well as the DNA-HMGB binding affinity are taken from refs (3) and (4). Comparisons to the data are shown in Figure 5G and 5H, using Eq. S9 as described in Supplementary Methods 7.
2. The linker length changes due to dispersion and the deduced nucleosome-HMGB binding affinity are determined from fits to the AFM sequential length data and Eq. S5 as described Supplementary Methods 4. Fits are shown in Figure 3G and 3H.
3. The average force required to disrupt the inner turn in the absence of protein and in saturating concentrations of HMGB are found along with the nucleosome-HMGB binding affinity are determined from fits to Eq. S6 as described in Supplementary Methods 5. Fits are shown in Figure 5B and 5C.

	$x^{\dagger}$ (nm)	k_o ($\times 10^{-3}$ s^{-1})	$G^{\dagger}$ (k_BT)
Arrays [1]	1.1 ± 0.1	1.2 ± 0.1	27 ± 1
Arrays [2]	0.9 ± 0.1	3.1 ± 0.4	26 ± 1
Arrays +Nhp6A [2]	0.6 ± 0.1	53 ± 4	24 ± 1
Arrays +Hmo1 [2]	0.6 ± 0.1	91 ± 9	23 ± 1

Supplementary Table S2. Results from force disruption experiments on nucleosome arrays.
OT experiments reveal thermodynamic evidence of core particle disruption.

1. Transition state distance ($\Delta x^{\dagger}$), barrier height ($G^{\dagger}$) and natural unwinding rates (k_o) are found from the fits as shown in the inset to Figure 4E to a dynamic force spectroscopy model and described in a previous study (6,7). Only the final unfolded nucleosome in each array was fit (so that A = 1). The calculated barrier height assumes a standard activation barrier pre-factor corresponding to overdamped conditions (10^9 s^{-1}) (8).
2. Transition state values are found in the fits to Eq. 1 as shown in Figure 4E and described in the text.

Fitting our data to the force spectroscopy model (inset of Figure 4E) gives results that do not match previous OT work, where k_0 was found to be ~10^{-6} s^{-1} (6), though these results match previous bulk studies (9). The discussion in the text focuses not on absolute values but on the changes in these parameters with the addition of HMGB proteins.

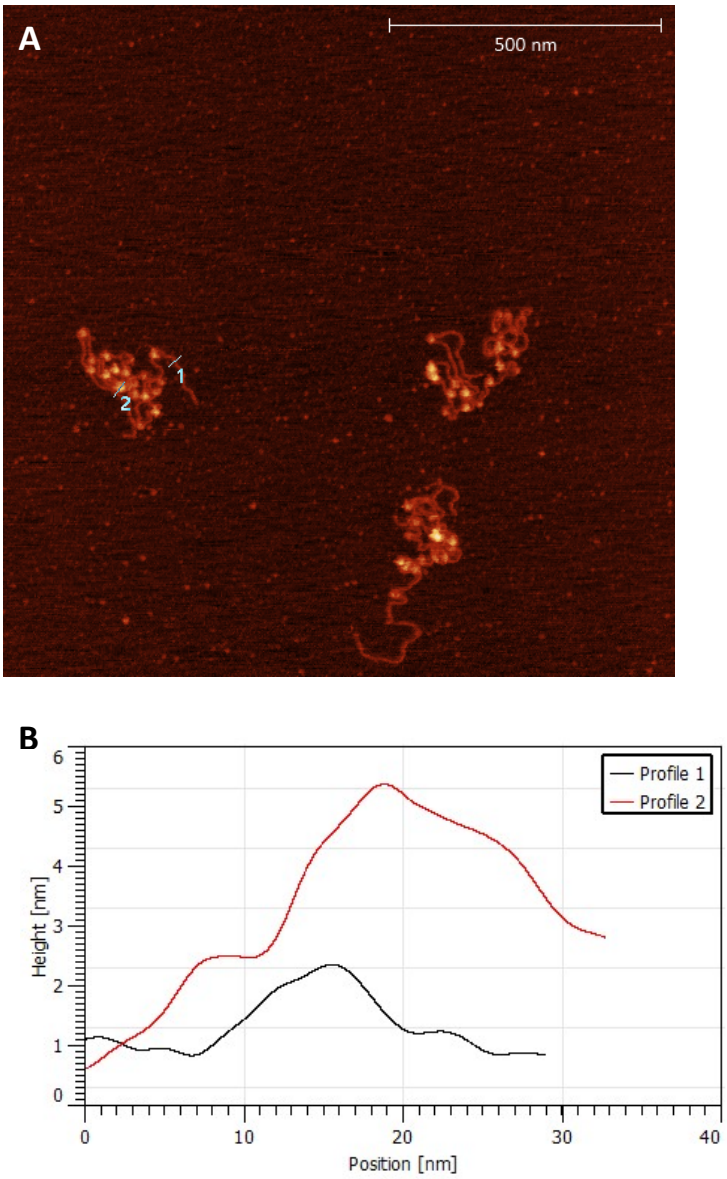

Supplementary Figure S1. Height profiles of AFM measurements.
(**A**) In this AFM image of three core particle clusters (each with 12 core particles), two lines are drawn and labeled (1, 2). Object image height is indicated on the scale to the right. (**B**) The measured height profiles for each line from (**A**) along the measured distance. The first profile (black line) cuts across the handle DNA and shows both height and width consistent with double stranded DNA, as convolved with the AFM tip. The second profile (red line) cuts across an identified nucleosome and shows an average height of 5 nm and full width of 15 nm, reasonably consistent with the known height of 6 nm and width of 11 nm of nucleosome core particles.

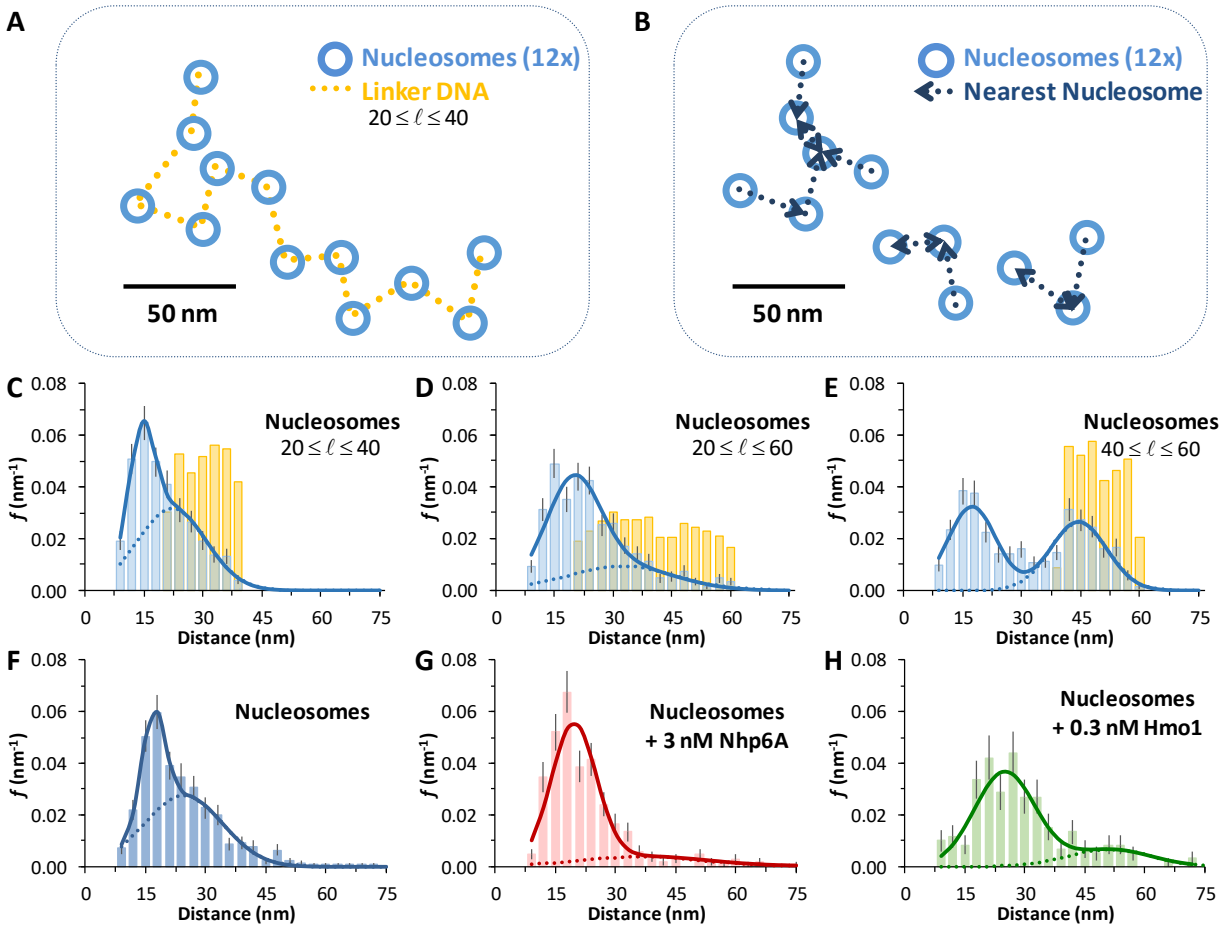

Supplementary Figure S2. Modeling unwinding in nucleosomal arrays.
Modeled distributions of unwound sequential distances compared to experiment. (**A**) A typical array of 12x nucleosomes, plotted to scale. Linker length are shown as straight lines in gold, simulated according to Supplementary Equations S2 and S3, for a length range between $20 \le \ell \le 40$ nm. (**B**) The measured nearest neighbor distances for the same array, shown as a blue arrow for each nucleosome. Several of the sequential linker lengths are not recovered (three of the twelve shown here), as a non-sequential nucleosome lies closer. (**C**) Histograms of modeled linker lengths (gold) and nearest neighbor distances (blue) for 42 random arrays as per the example in (**A**) and (**B**) (N = 504). Similar sets may be generated, but with the linker range of (**D**) $20 \le \ell \le 60$ nm and (**E**) $40 \le \ell \le 60$ nm. Dual Gaussian fits (solid blue lines), described in Supplementary Methods S1, give sequential nearest neighbor lengths (dotted blue lines) of (**C**) 22 ± 3 nm, (**D**) 32 ± 4 nm and (**E**) 44 ± 3 nm. These modeled data sets are compared to experimental data for (**F**) nucleosomes, (**G**) nucleosomes with 3 nM Nhp6A and (**H**) 0.3 Hmo1. The model parameters of (**C**) match the actual data of (**F**) well, indicating some heterogeneity in the linker length even with no protein present. The model of (**D**) but not (**E**) matches the appearance of both (**G**) and (**H**), showing both an increase in both unwinding and heterogeneity as protein is added.

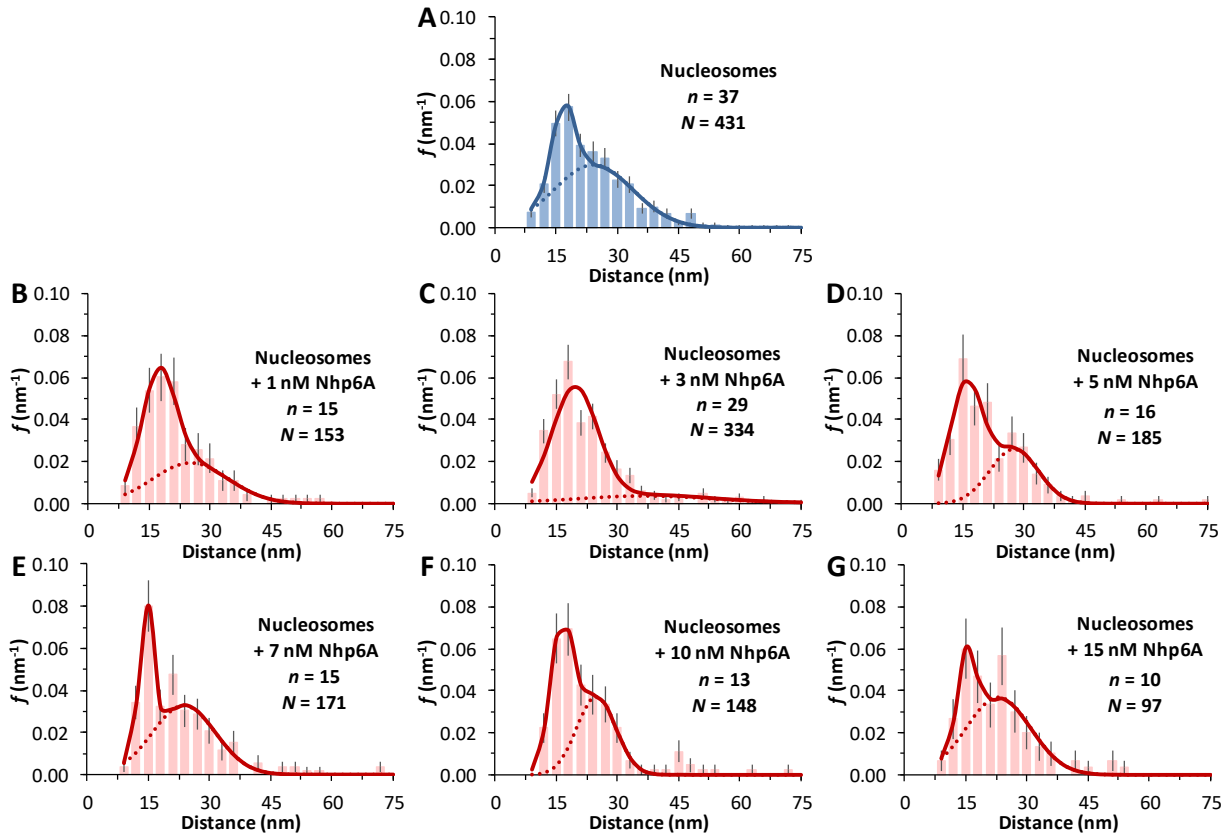

Supplementary Figure S3. Fitting distance profiles in varying Nhp6A concentrations.
Fitted measurements of nearest neighbor distances for (**A**) nucleosomes and increasing concentrations of Nhp6A; (**B**) 1 nM, (**C**) 3 nM, (**D**) 5 nM, (**E**) 7 nM, (**F**) 10 nM and (**G**) 15 nM. Histograms formed from nearest neighbor distances from the indicated number of arrays (*n*) and total number of identified nucleosomes (*N*). Solid lines are fits to double Gaussian function of Supplementary Methods 1 (where $0.5 < \chi_v^2 < 2$). Mean distances (μ) are found and shown with fitted error in Figure 3. The dotted line indicates the distribution of distances identified as nearest sequential neighbor.

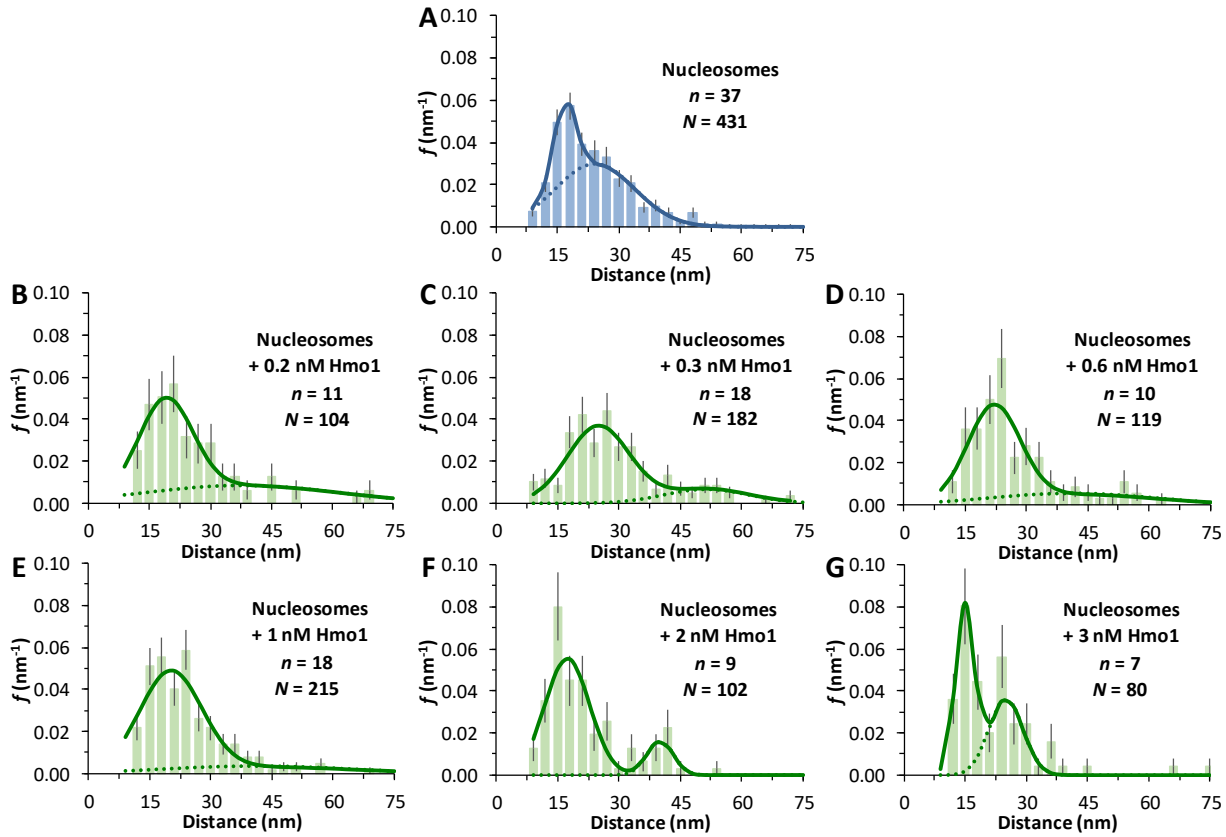

Supplementary Figure S4. Fitting distance profiles in varying Hmo1 concentrations.
Fitted measurements of nearest neighbor distances for (**A**) nucleosomes and increasing concentrations of Hmo1; (**B**) 0.2 nM, (**C**) 0.3 nM, (**D**) 0.6 nM, (**E**) 1 nM, (**F**) 2 nM and (**G**) 3 nM. Histograms formed from nearest neighbor distances from the indicated number of arrays (*n*) and total number of identified nucleosomes (*N*). Solid lines are fits to double Gaussian function of Supplementary Methods 1 (where $0.5 < \chi_v^2 < 2$). Mean distances (μ) are found and shown with fitted error in Figure 3. The dotted line indicates the distribution of distances identified as nearest sequential neighbor.

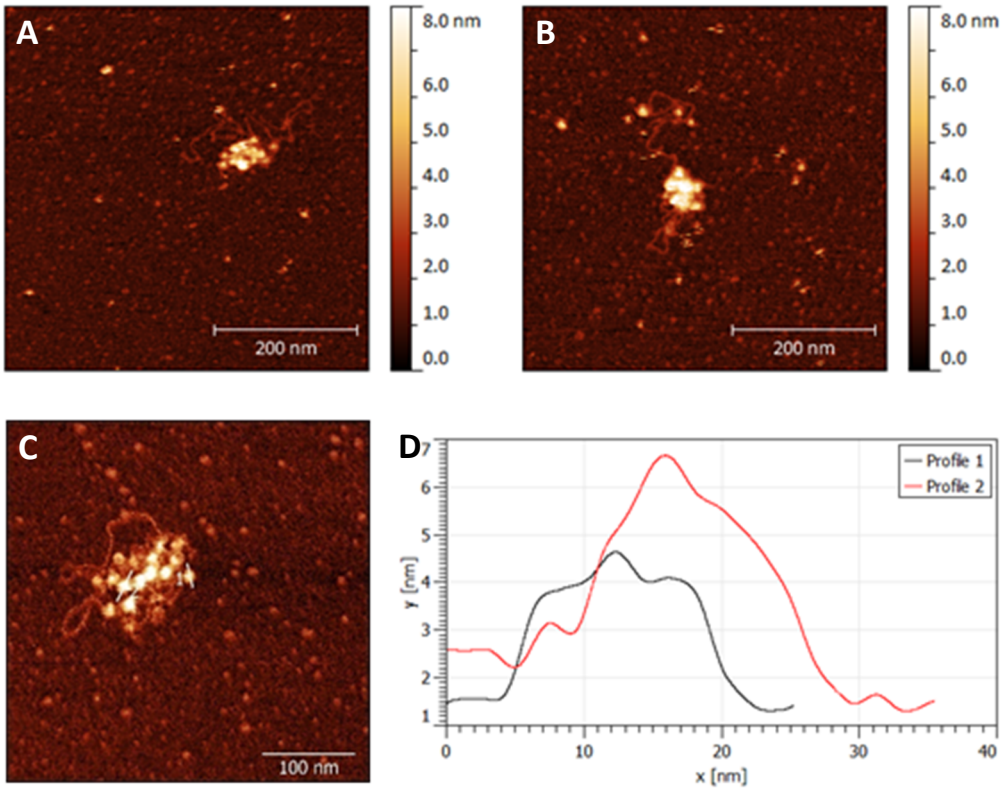

Supplementary Figure S5. Strong compaction at high concentrations of Nhp6A.
(**A, B**) In 20 nM Nhp6A, core particles are very strongly compacted, as the twelve core particles are barely discernable and lie side by side. Nearest neighbor distances cannot be determined in these images. The concentration of 20 nM, however, is well below the known K_d of 70 nM for Nhp6A binding to double-stranded DNA (3). (**C, D**) Height profiles for an isolated core particle (profile 1) and a compacted region (profile 2) show differences in both height and total profile area under the curve that indicate partial stacking of core particles.